

The BHK Color Diagram: a New Tool to Study Young Stellar Populations

Daniel Devost¹

Département de physique and Observatoire du mont Mégantic, Université Laval, Québec,

QC G1K 7P4, Canada

Space Telescope Science Institute, 3700 San Martin Drive, Baltimore, MD 21218 USA

Received 15 Dec. 1998; accepted 30 Mar. 1999

AJ accepted

arXiv:astro-ph/9904019v1 1 Apr 1999

¹Visiting astronomer, Canada-France-Hawaii Telescope, which is operated by the National Research Council of Canada, the Centre National de la Recherche Scientifique of France, and the University of Hawaii.

ABSTRACT

A new method to derive age differences between the various super star clusters observed in starburst galaxies using the two color diagram (B–H) *vs* (H–K) is presented. This method offers a quick and easy way to differentiate very young and intermediate age stellar populations even if data on extinction are unavailable. In this case, discrimination of regions younger and older than 4 Myr is feasible. With the availability of data on extinction, the time resolution can be improved significantly. The application of the method to the starbursting system Arp 299 is presented. The validity of the method is confirmed by comparing the equivalent width of the H α line with the chronological map of the northern part of NGC 3690.

Subject headings: Stars: formation — Infrared: Galaxies: interacting Arp 299 — Galaxies: individual NGC 3690 — Galaxies: starburst — Galaxies: photometry

1. INTRODUCTION

Prior to the pioneering study of “flashing galaxies” by Searle, Sargent , & Bagnuolo (1973), galaxy evolution was thought to be a smooth, exponentially decaying process lasting several billion years. The discovery of a significant population of galaxies actively forming stars dramatically changed this picture (Harris & van den Berg 1981; Seiden & Gerola 1982; Schweizer 1986; Burstein 1986; Kumai, Basu , & Fujimoto 1993). Many galaxies are now known to experience a series of episodes of enhanced star formation during their lifetime, especially through merging events (Schweizer 1986; Zepf, Geisler, & Ashman 1994), but also following the formation of a bar (Phillips 1996; Martin & Friedli 1997).

Although known to be very important in the evolution of galaxies, the star formation process is usually poorly accounted for in galactic evolution models. “Recipes” (e.g. Kennicutt 1998) are provided to account for the global characteristics of the star formation rate versus the interstellar medium (ISM); those are derived from the global or azimuthally averaged properties of observed galaxies while star formation is a local phenomenon. Little is known about the local aspects of the star formation process. The way the star formation propagates, the dynamics of the star formation, and its relation to the physical properties of the ISM are usually parameterized as a percolation phenomenon (Mueller & Arnett 1976; Gerola & Seiden 1978; Seiden, Schulman , & Gerola 1979; Seiden & Gerola 1982) or regulated by feedback or porosity (Navarro & Steimetz 1997; Silk 1997). All are ad-hoc parameterizations of a very complicated process.

One of the most difficult tasks in the quantification of the star formation process is to assign precise ages to star forming regions. Starburst galaxies are ideal objects to study the local properties of various star forming regions and their effects on the properties of a galaxy. Starbursts form many compact ($\sim 2\text{-}5$ pc), luminous and blue ($-11 > M_{UV} > -18$) super star clusters (SSC; Meurer et al. 1995) that radiate tremendous amounts of

light in all wavebands. Also, a reasonable fraction of this light can easily ionize many atoms to the first or second stage of ionization, while the high supernovae rate associated with starbursting regions excites and ionizes elements to even higher stages.

These characteristics of starbursting regions provide the opportunity to study the physical properties of the gas. The knowledge of the gas properties is essential if one wants to constrain the parameters involved in the quantification of the star formation process. Several parameters of a stellar population other than age, can cause a variation of the integrated magnitude and colors of a SSC. Extinction, metallicity and the mass of stars formed at present or at any given time by the cluster are all factors that can affect its observed characteristics. It is a difficult task to disentangle which parameter or combinations of parameters cause the differences in the observed integrated magnitudes and colors of stellar clusters. For example, a young cluster embedded in dust can be mistaken for an old, unreddened cluster.

Nevertheless, with appropriate tools, the effect of these various parameters can be separated. In this paper, I will show that the extinction degeneracy can be lifted by a reasonable amount by studying the SSC integrated light with the (B–H) vs. (H–K) two color diagram (BHK diagram). I discuss in §2 the main physical arguments that support this choice of colors and I propose an application of the method to the interacting system Arp 299 in §3.

2. CHRONOMETRY WITH THE BHK DIAGRAM

2.1. MODELING

Figure 1 shows the theoretical behavior of the BHK colors for an instantaneous coeval burst of star formation forming $10^6 M_{\odot}$ of stars ranging from 1 to $120 M_{\odot}$ according to a

Salpeter initial mass function using the models of Leitherer et al. (1999). These models are implemented with the new set of stellar evolution models of the Geneva group. For masses of $12 - 25 M_{\odot}$ (depending on metallicity) and above, the Leitherer et al. models are using evolutionary tracks with enhanced mass loss of Meynet et al. (1994). The tracks of Schaller et al. (1992), Schaerer et al. (1993a, 1993b), and Charbonnel et al. (1993) with standard mass loss are used between 12 and $0.8 M_{\odot}$. Atmosphere models are from Lejeune, Buser, & Cuisinier (1997) for stars which are not in a Wolf-Rayet phase. Wolf-Rayet stars are modeled with the atmospheres of Schmutz, Leitherer, & Gruenwald (1992). A discussion of the uncertainties related to the modeling technique can be found in Leitherer et al. (1999).

A modification to the models was necessary since stellar evolution models fail to reproduce the red supergiants (RSG) features at low metallicities. As the study of Origlia et al. (1998) pointed out, the low metallicity models does not reproduce the CO 1.62μ and CO 2.29μ indices as well as the J–K colors of a selected sample of LMC young clusters. However, they pointed out that if the fraction of time spent as a RSG during the core-helium phase is forced to at least 50 % and if the RSG temperature is maintained to less than 4000 K, the models agrees well with the observations. Our modeling technique was modified according to this prescription.

The calculated paths on the BHK diagram of Figure 1 are for metallicities of $0.05 Z_{\odot}$ and Z_{\odot} and no extinction is shown. In the next three sections, I discuss how different fundamental parameters like the metallicity, extinction, dust emission and nebular emission can affect the locus of the observed points on the BHK diagram and why the B, H and K colors are the best choice for this type of study.

2.2. THE EFFECT OF METALLICITY

For a single metallicity, the colors are distributed in a u-shaped form (see Figure 1), where two different branches can be easily seen. The “young branch” runs almost diagonally from the right to the left of the diagram. The light originating within a young starbursting region may be dominated by massive O stars ($\sim 80\%$) and nebular emission ($\sim 20\%$) in the B band, while in the H and K bands, the nebular emission may contribute up to as much as ~ 70 to 85% of the total flux. As the nebular emission becomes negligible with the massive O stars evolving to become red supergiants, a turnoff occurs in the integrated colors. The color path then takes the “old branch”, a path that mainly runs along the (B–H) axis. After 10 Myr, the color path turns around and follows the old branch. This behavior causes a degeneracy between regions aged between 6 and 10 Myr and those aged between 10 and 50 Myr. As we will see in section §3.2, this degeneracy can easily be lifted with spectroscopic data. After 50 Myr (not shown in Figure 1), the colors do not change significantly and the evolutionary path remain in the same region than the 50 Myr point.

Models in Figure 1 also show that an increase in the metallicity of the SSC produces a different behavior of the colors (Figure 1). This behavior can be mistaken for an age change. However, known abundance properties in galaxies help; the metal distribution in small starburst galaxies shows no or very shallow abundances gradients (Kobulnicky & Skillman 1997; Devost, Roy, & Drissen 1997; Kobulnicky 1998). The two metallicity tracks shown in Figure 1 would correspond to an extreme gradient of several dex kpc^{-1} ; such a change in metallicity between two close SSC belonging to the same galaxy is most unlikely. Thus, the tracks of a group of SSC from the same galaxy should show parts falling on the same track on the BHK color diagram, in the absence of extinction.

2.3. THE EFFECT OF EXTINCTION AND DUST EMISSION

The extinction vector on the BHK diagram is more or less parallel to the old branch since $E(H-K) \sim 0.1 E(B-H)$. This alignment is the key point to extinction correction. Extinction will move any points in the old or in the young branch along a vector that is parallel to the old branch. This has two important advantages. First, the structure of the old branch will still be recognizable since its alignment with the extinction vector will prevent its spread by local extinction differences. Global dereddening is then possible by fitting together the theoretical old branch path and the observed old branch structure. The second benefit is that extinction of points belonging to the young branch will not be moved to the old branch by extinction. An example of such a degeneracy is given in Figure 2. This two color diagram plots the behavior of the $(B-J)$ vs. $(J-H)$ with the same model parameters as in Figure 1 for solar metallicity stars. We can see that the young and old branches are still there but extinction of points belonging to the young branch will cross the path of the old branch, making the distinction between an age and an extinction effect almost impossible. Also, the misalignment of the any of the two branches with the extinction vector causes a spreading of the points by local extinction differences and it is very unlikely that the structure of any of the two branches will be conserved.

Warm dust emission will also modify the behavior of the observed infrared colors of SSCs. Satyapal et al. (1995) showed that warm and hot dust emission contaminates only the K band by adding at most 20% to its total flux. Thus, hot dust will make the observed points redder by a factor of at most 0.2 mag along the $(H-K)$ axis. This value is not high enough to produce a degeneracy between the young and old branches but will move the points belonging to the young branch further to the red thus enhancing the difference between the two branches.

2.4. THE EFFECT OF NEBULAR LINES

Nebular emission is also a factor that can produce degeneracies. In the infrared bands, the main contribution comes from the $\text{Br}\gamma$ emission line which contaminates the K band. The models of Leitherer et al. (1999) show that for a continuous burst of star formation, the equivalent width of the $\text{Br}\gamma$ line decreases from $\sim 500 \text{ \AA}$ when the burst is younger than 3 Myr to less than 100 \AA when the burst is older than 4 Myr. This means that the $\text{Br}\gamma$ nebular line will add $\sim 0.12 \text{ mag}$ to the K band light when the cluster is younger than 3 Myr and less than 0.02 mag when the cluster is older than 4 Myr. The implications for the BHK diagram is that the $\text{Br}\gamma$ emission line pushes the points belonging to the young branch further to the red and thus, once again, enhancing the difference between the old and the young branch.

The nebular component in the optical part of the spectrum is much more important. The hydrogen and the oxygen lines can make an important contribution to the measured flux and produce unwanted degeneracies. The $\text{H}\alpha$ line contaminates the R band filter while the $\text{H}\beta$ and $[\text{O III}](\lambda\lambda 5007, 4959)$ can make significant contribution to the V band flux. However, the B band is affected to a lesser degree than the V band filter since the transmission of the B filter at the wavelength of these lines is about 15% less than the transmission of the V filter. Also, even moderate redshifts will shift these lines further into the V waveband. So for our purpose, the B band filter is minimizing the contamination by the nebular lines.

2.5. TIME RESOLUTION

The considerations outlined in the latter sections restrict the choice of colors to B, H and K. The alignment of the old branch with the extinction vector as well as the effects of

dust emission and nebular line emission are strong arguments in favor of this choice. The achievable time resolution of this method is mainly limited by the extinction differences from one cluster to the other. However, even with no data on extinction, discrimination of regions younger and older than 4 Myr is still feasible. The age determination in this case is solely based on the color differences between the old and young branches. Nevertheless, if the exciting stars are not completely embedded in dust and are themselves visible in the optical domain, nebular lines ratios measured from line-of-sight spectra to the stellar knots allow a first-order correction. In such a situation, extinction correction using the Balmer lines decrement helps to lift a good part of the (B–H) degeneracy, then allowing age determinations with a time resolution limited by the assumed dust and gas properties.

Uncertainties in the dust modeling mainly comes from the assumptions made on its spatial distribution. Dust extinction can be modeled assuming a foreground uniform screen or a clumpy layer in front the extinguished stellar population, or assuming that the dust is mixed within the stellar population (Natta & Panagia 1984, Calzetti, Kinney & Storchi-Bergmann 1994). Observations of starburst galaxies seem to rule out dust and stars mixed internally. The intrinsic nature of a starburst, e.g. the high stellar winds and the frequent supernovae explosions, may in fact favor the foreground screen geometry (Calzetti 1998). However, very young clusters can be mixed with dust and suffer very high extinction (Calzetti et al. 1997). This type of regions maybe missed by the BHK diagram since they will not be detected in the broad band images.

Nevertheless, for the regions detected in the broad band images, the worst case scenario would be to make a correction for extinction in the BHK diagram for a clumpy medium using the foreground screen approximation. In that case, for a value of $A_V \sim 2$, the difference between assuming a foreground screen and a clumpy dust distribution produces a color difference $\Delta E(B-V)$ of 0.35. This produces some uncertainty on the dating of the

burst, the magnitude of which depends on where the burst is along its evolutionary track in Figure 1. A small change in (B-H) produces a larger time error for a 1 Myr old burst than it does for a 6 Myr old burst.

The uncertainty on the dating of the burst will also be affected by the model used to correct for extinction. There is a fair amount of evidence that the extinction derived from the stellar continuum is systematically less than that derived from the nebular gas (e.g. $H\alpha/H\beta$ ratios). This seems to indicate that the dust is mostly mixed with the gas, and the stars are mostly seen through regions of lower optical depth. However, a higher degree of accuracy can be reached if the ratio of the extinction derived from the stellar continuum to the value derived from the nebular gas is known. This ratio is believed to be between 2 and 3 for starburst galaxies (Meurer et al. 1995, Calzetti, Kinney & Storchi-Bergmann 1994). Using the extinction law of Kinney et al. (1994) to scale between $\Delta E(B-V)$ and $\Delta(B-H)$ and a conversion factor between the continuum extinction and the nebular gas extinction of 2.5, the error produced by the assumed spatial geometry translates in the BHK diagram to values of ~ 1.4 Myr along the old branch and ~ 2.0 Myr along the young branch. Changing the conversion factor between the continuum extinction and the Balmer extinction does not change significantly the error estimate on the age determination.

For ages ranging from 10 to 50 Myr, the time resolution has a value worse than 11 Myr. The type of resolution derived for these ages or greater, is incompatible with the purpose of dating star forming regions to infer the properties of the star formation process. This means that the BHK diagram can only be useful to trace star formation to a reasonable resolution for regions that are younger than 10 Myr.

2.6. A DOUBLE BURST MODEL

I explored the behavior in the BHK diagram of a model that forms star clusters in two bursts. The super star cluster A in NGC 1569 maybe the result of such a burst. González Delgado et al. (1997) found that in this cluster, red supergiants features as well as Wolf-Rayet features were present and suggested a double burst scenario to explain the coexistence of these features within the same cluster. However, the detection of red supergiants and Wolf-Rayet features within the same spatial location may also be caused by the alignment of two clusters along the same line of sight (De Marchi et al. 1997).

I modeled the BHK colors of two identical unresolved bursts occurring 1 Myr (double burst model 1) and 3 Myr (double burst model 2) apart. The integrated colors of the double burst were derived using:

$$(B - H)_{DB} = (B - H)_O - 2.5 \log\left(\frac{1+A}{1+B}\right)$$

where,

$$A = 10^{0.4(M_{B_O} - M_{B_S})} \quad \text{and} \quad B = 10^{0.4(M_{H_O} - M_{H_S})}$$

Subscript DB means double burst, subscript O relates to the original burst and subscript S relates to the second burst. M_{B_O} , M_{B_S} , M_{H_O} and M_{H_S} are the absolute B and H magnitudes of the original and second burst respectively. The same algorithm was used for the (H–K) color. The physical parameters of the model are the same as the solar metallicity burst of Figure 1 and no chemical evolution occurs between the two bursts.

The results are compared to the single burst model in Figure 3. The paths of the single burst and the double burst model 1 are almost identical but differ significantly between the single burst and the double burst model 2. When both bursts are at young age ($t < 4$ Myr)

the age estimate is not affected. At intermediate age, a shift occurs in the (B–H) color so that a 5 Myr old single burst can be mistaken for an 6 Myr old double burst (model 2; Figure 3). This means that if a single burst approximation is made when the studied cluster formed in two bursts separated by 3 Myr, the time estimate can be altered at ages between 6 and 10 Myr by a value of 1 to 2 Myr. However, if the two bursts are resolved and occurred at different spatial locations, each stellar populations will be given an age by the BHK diagram that will not be affected by the double burst scenario.

3. A TEST CASE: Arp 299

I have tested the BHK diagram method of chronometry by exploring the SSCs in the interacting system Arp 299. This system includes two galaxies; NGC 3690 and IC694. The assumed distance to this object is 42 Mpc (Nordgen, et al. 1997; $H_0 = 75 \text{ km s}^{-1} \text{ Mpc}^{-1}$). Several UV bright young SSCs (Meurer et al. 1995) are present as well as bright infrared sources. With their K band image, Wynn-Williams et al. (1991) identified four bright infrared sources belonging to the whole system, three of which are associated with NGC 3690 and one associated with IC 694. More recently, Satyapal et al. (1997) established that the light coming from Arp 299 can be entirely explained by a starburst model. I will show how an age determination of the various sources with the BHK diagram gives insight into the star formation history of Arp 299.

3.1. OBSERVATIONS AND DATA REDUCTION

Observations of Arp 299 were obtained during three different observing runs. First, wide band BVRI images were obtained at the 1.6 meter telescope of the Observatoire du mont Mégantic (OMM) in March 1996. The detector was the Thompson THX 1024×1024

CCD with pixel size of 19μ and a plate scale of $0.31'' \text{ pix}^{-1}$. The JHK band images were taken with the Canada-France-Hawaii Telescope (CFHT) in January 1997 using the infrared camera MONICA (Nadeau et al. 1994). Spectroscopy of Arp 299 was also performed at the CFHT with MOS-ARGUS, a fiber optics system that allows 2-D spectroscopy with a $\sim 12'' \times 10''$ field of view and sampling fiber apertures of $0.4''$. The detector used was the STIS2 $2K \times 2K$ thin CCD with 21μ pixels.

3.1.1. Wide band images

For optical imaging analysis, bias, flatfield and dark images were taken during the same night the observations were performed. The corresponding correction was made for each image of Arp 299. Flux calibration was achieved with Feige 56. Exposure times and other relevant information about the observing run are listed in Table 1. Bad pixels were removed by interpolation. Images in one filter were combined using a combination algorithm to eliminate the signature of the cosmic rays and to increase the signal-to-noise (S/N) ratio. The mean FWHM of the point-spread function as measured from stars in the field of the four combined images is $\sim 1''$. The sky conditions the night of the observations allowed reliable photometry. The images were then aligned together using field stars. All the successive image reduction steps were performed with IRAF.

The second set of observations was done at the CFHT in the J, H, and K bands with the IR camera MONICA (Nadeau et al. 1994) at the f/8 focus on January 20 1997 (Table 1). The images were corrected for flatfield and dark current. The flux calibration was made with the IR UKIRT standard stars FS2, FS21, and FS25. Bad pixels were corrected with a mask. In each band, four images were combined using a rejection routine to raise the S/N ratio and remove the cosmic ray signature. The images were aligned using point sources common to the three wavebands. During the observations, the seeing was $0.7''$.

Once again, the sky was clear and allowed for reliable photometric calibration. Most of the data reduction steps were performed using software developed by the Montreal group (D. Nadeau). Steps not requiring this software were done with IRAF.

Both set of images were calibrated by deriving the zeropoints of the magnitude system from the flux of their respective standard stars. With this type of calibration, there are two main sources of uncertainty in the measured magnitudes. One comes from the uncertainty on the value of the zeropoints and the other one comes from photon noise. However, as we will see in §3.2, only the bright points were used for analysis so the photon noise is negligible. In this case, the error on the derived magnitudes only comes from the zeropoints uncertainty which is of the order of 0.1 in B and H and 0.2 in K which translates to an error of 0.15 in (B–H) and 0.22 in (H–K) (see the error bars of Figure 5).

The optical and infrared images were then scaled together using the I band image of the OMM and the J band image of the CFHT. Sources common to both images were used as reference points.

3.1.2. 2-D Spectroscopy

Observations with the 2-D spectrograph MOS-ARGUS were done during the nights of February 27 to March 1 1998 with the B600 grism and the STIS II CCD at the f/8 focus of the CFHT. The spectral range is from 3600 to 7000 Å and the dispersion is 2.2 Å pix⁻¹ (Table 1). MOS-ARGUS is a fiber optic spectrograph that puts 594 fibers arranged in an hexagon shaped bundle that allows for the collection of that many spectra per exposure. The fibers are grouped in 25 rows that contain a number of fibers increasing from 18 to 30, giving a maximum field of view of 12" × 10". Each fiber sampled an aperture of 0.4" which corresponds to a scale of 80 pc at the assumed distance of 42 Mpc. Data reduction was

done with IRAF procedures that I specially developed for reduction of the MOS-ARGUS data. A monochromatic image reconstruction software was built using the software package IDL. All spectra were bias and flatfield corrected. Special care was taken to correct for fiber transmission and wavelength response.

3.2. ANALYSIS AND RESULTS

Figure 4 shows the K image of Arp 299 labeled with the conventional symbols of Wynn-Williams et al. (1991). The data of Mazzarella & Boroson (1993) shows surprisingly uniform oxygen abundances at about a third solar all over the galaxy. The logarithmic extinction differences at $H\beta$ between the various regions they studied are of the order of $\Delta c = 0.2 - 0.3$ which corresponds to a $\Delta(B-H)$ of 0.6.

Figure 5 compares the models with the observed color of the $0.7'' \times 0.7''$ (150×150 pc) aperture points in the binned images; I chose a threshold in absolute M_B and M_K magnitude to have only points brighter than -10 and -14 , respectively. Plotting the observed points instead of the integrated magnitudes ensures that most of the spatial information is extracted from the observations since a single resolution element covers 150 pc. Ideally, one would want to be able to resolve each individual cluster and derive the integrated colors. This would minimize the probability of having more than one burst within one aperture and give the most reliable spatial information. However, such resolution are unreachable from the ground for Arp 299.

The parameters of the model in Figure 5 are the same as those shown in Figure 1 with the exception that Figure 5 was made using the stellar evolutionary tracks of metallicity 0.40 solar. Also, dust emission corresponding to 0.2 mag in K was added to the original evolutionary track in order to compare the data with more realistic models. The track with

dust emission is then shifted of a value of 0.2 magnitude to the red along the x axis. The best global fit of the theoretical tracks to the data gives an extinction correction $E(B-V) = 0.16$, which is in agreement with the value derived by Meurer et al. (1995) and with the value inferred from the data of Mazarella & Boroson (1993).

The ages were determined in the following way. All the points that fall between the two old branches (see Figure 5) but with $(B-H) < 1.2$ are considered to be aged between 4 and 7 million years. All the points with $(B-H) > 1.2$ are given an age of 7 to 10 Myr. Notice that the points belonging to this part of the diagram could be aged between 10 and 50 Myr (see §2.2) but the nebular analysis (next paragraph) shows that this is not the case. The value of $(B-H) = 1.2$ is set by the uncertainty on the color that is caused by the measured extinction differences since in this case, extinction is the major source of uncertainty. All the points that lie outside the two tracks are labeled to be younger than 4 Myr. These points belong to the young branch and have been shifted to this part of the diagram by extinction, dust emission and nebular line emission. The derived chronological map is shown on Figure 6. This map shows that: *i*) objects C, B1 and A are the youngest of the system; *ii*) a region to the south west of object A and one to the south of object C, are approximately 3 Myr older and *iii*) object B2 and a region located to the south west of object A are the oldest regions of Arp 299.

A further test of the validity and of the limitations of this approach can be made with the 2-D spectroscopy of MOS-ARGUS. The equivalent width of $H\alpha$ ($EW(H\alpha)$) is known to be a very strong function of age, because it traces very young star forming regions (Leitherer et al. 1999). However, it cannot be used give precise ages due to geometrical considerations (Devost, Roy, & Drissen 1997). Nevertheless, a young region should show up as a high and peaked region in $EW(H\alpha)$. Figure 7 shows a contour map of $EW(H\alpha)$ for NGC 3690, derived from MOS-ARGUS spectroscopic observations superposed to the wide

R band image. The contours indicate a direct correlation between object C and the highest $EW(H\alpha)$ region located to the north of the image. This spatial correlation between the stellar light and the nebular light is very distinctive of young regions. The region with high $EW(H\alpha)$ located to the west of B2 is also most interesting. This region has a high value of $EW(H\alpha)$ but has a very low underlying continuum. Careful examination of the HST UV image of Meurer et al. (1995) shows that this region doesn't contain any UV bright sources and no sources are detected in our B or in our K band image. This lack of continuum light means that this region is probably very young and still buried in dust. The continuum light is heavily extinguished so this region is not detected in the broad band images. Such a region is then missed by the BHK diagram and $EW(H\alpha)$ is needed to locate them.

Region B2, also seen in the wide R band image, is an older object according to $EW(H\alpha)$ since it is more extended and has a much smaller value of $EW(H\alpha)$. These results also confirm those obtained previously with the BHK diagram. Nevertheless, the BHK diagram analysis alone cannot assign a precise age to region B2 because the evolutionary paths of Figure 5 are degenerate for ages between 7 to 10 Myr and 10 to 50 Myr. The $EW(H\alpha)$ is necessary to lift this degeneracy. The models of Leitherer et al. 1999 shows that the *integrated* $EW(H\alpha)$ has a value of $\sim 1 \text{ \AA}$ at 14 Myr and rapidly becomes undetectable as the stellar population becomes older. The value of the *surface* $EW(H\alpha)$ derived in Figure 7 ($\sim 5 \text{ \AA}$) around object B2 is too high for this object to be in the 10 - 50 Myr age range so this region must be in the 7 -10 Myr age range.

4. DISCUSSION AND CONCLUSION

The clear distinction between the two branches seen in the BHK diagram allows for reliable discrimination between regions younger than 4 Myr and those older than this age, even if no data on extinction is available. The BHK diagram clearly categorizes three (A,

B1, C) of the four infrared sources of Arp 299 as being very young (< 4 Myr). Also, with the help of the $\text{EW}(\text{H}\alpha)$, region B2 is identified as being between 7 and 10 Myr. The correlation between the highest $\text{EW}(\text{H}\alpha)$ region and region C, labeled young from the BHK diagram analysis, supports the validity and usefulness of this diagram as a tool for determining the relative ages of young stellar populations in starbursting regions. Also, a region located to the west of object B2 has also a high value of $\text{EW}(\text{H}\alpha)$ and is missed by the BHK diagram. Clearly, very young regions still buried in dust are very likely to be missed by the diagram since they are not detected in broad band images.

The nebular analysis is found to be a useful complementary tool to the BHK diagram. In addition to the complementary use of the $\text{EW}(\text{H}\alpha)$, data on extinction with any of the Balmer lines allows to achieve a better time resolution. This is essential to derive more precise star formation properties since extinction is the main contributor to the uncertainty on the time labeling. In the case of Arp 299, the extinction differences inferred from the data of Mazzarella & Boroson (1993) limits our resolution to ~ 3 Myr. Also, their longslit data only sampled a small part of the galaxy and the extinction from the unsampled regions is unknown. The use of 2-D spectroscopy will reduce considerably the uncertainty on extinction. Corrections using the $\text{H}\alpha/\text{H}\beta$ line ratio will lower the time resolution down to the limit imposed by the uncertainty of the assumed dust model for extinction which I have shown to be of the order of 1.5 to 2 Myr.

I thank Gilles Joncas and René Doyon who kindly obtained the infrared images of Arp 299 at CFHT. Discussions with Jean-René Roy, Carmelle Robert and Claus Leitherer were most helpful. The comments of D. Calzetti were appreciated. I would also like to thank the anonymous referee whose suggestions and comments significantly helped to improve the paper. This research was supported by the Natural Sciences and Engineering Research Council of Canada, by FCAR of the Government of Québec and by the STScI DDRF. I am

thankful to the STScI, and in particular to Claus Leatherer, for hospitality during my stay when part of this work was accomplished.

REFERENCES

- Burstein, D. 1986, in *Nearly Normal Galaxies*, ed. S. Faber, (New York: Springer), 47
- Calzetti, D. 1998, in *XXXIIIrd Rencontres de Moriond on Dwarf Galaxies*, eds. T. X. Thuan, C. Balkowski, V. Cayatte, & J. Tran Thanh Van, in press
- Calzetti, D., Kinney, A. L., & Storchi-Bergmann, T. 1994, *ApJ*, 429, 582
- Calzetti, D., Meurer, G. R., Bohlin, R. C., Garnett, D. R., Kinney, A. L., Leitherer, C., Storchi-Bergmann, T. 1997, *AJ*, 114, 1834
- Charbonnel, D., Meynet, G., Maeder, A., Schaller, G., & Schaerer, D. 1993, *A&AS*, 101, 415
- Devost, D., Roy, J.-R., & Drissen, L. 1997, *ApJ*, 482, 765
- De Marchi, G., Clampin, M., Greggio, L., Leitherer, C., Nota, A., & Tosi, M. 1997, *ApJ*, 479, 27
- Gerola, H, & Seiden, P. E. 1978, *ApJ*, 223, 129
- González Delgado, R. M., Leitherer, C., Heckman, T., Cerviño, M. 1997, *ApJ*, 483, 705
- Harris, W. E., & van den Berg, S. 1981, *AJ*, 86, 1627
- Kennicutt, R. C. Jr. 1998, *ApJ*, 498, 541
- Kinney, A.L., Calzetti, D., Bica, E. & Storchi-Bergmann, T. 1994, *ApJ*, 429, 172
- Kobulnicky, C. 1998, in *Abundance Profiles: Diagnostic Tools for Galaxy History*, ASP Conf. Ser. Vol. 147, eds. D. Friedli, M. Edmunds, C. Robert, & L. Drissen (San Francisco: ASP), 108
- Kobulnicky, C., & Skillman, E. D. 1997, *ApJ*, 489, 636
- Kumai, Y., Basu, B., & Fujimoto, M. 1993, *ApJ*, 438, 702

- Leitherer, C., Schaerer, D., Goldader, J. D., González Delgado, R. M., Robert, C., Kune, D. F., de Mello, D. F., Devost, D., & Heckman, T. M. 1999, ApJS in press.
- Lejeune, T., Buser, R., & Cuisinier, F. 1997, A&AS, 125, 229
- Martin, P., & Friedli, D. 1997, A&A, 326, 449
- Mazzarella, J. M., & Boroson, T. A. 1993, ApJS, 85, 27
- Meynet, G., Maeder, A., Schaller, G., Schaerer, D., & Charbonnel, C. 1994, A&AS, 103, 97
- Meurer, G. R., Heckman, T.M., Leitherer, C., Kinney, A., Robert, C., & Garnett, D. A. 1995, AJ, 110, 2665
- Mueller, M. W., & Arnett, W. D. 1976, ApJ, 210, 670
- Natta, A., & Panagia, N. 1984, ApJ, 287, 228
- Navarro, J. F., & Steimetz, M. 1997, ApJ, 478, 13
- Nadeau, D., Murphy, D. C., Doyon, R., & Rowlands, N. 1994, PASP, 106, 909
- Nordgren, T. E., Chengalur, J. M., Salpeter, E. E., & Terzian, Y. 1997, AJ, 114, 77
- Origlia, L., Goldader, J. D., Leitherer, C., Schaerer, D., & Oliva, E. 1998, ApJ, submitted
- Phillips, A.C., 1996, in Barred Galaxies, eds. R. Buta, B. Elmegreen, & D. Crocker (San Francisco: ASP), 44
- Satyapal, S., Watson, D. M., Pipher, J. L., Forrest, W. J., Coppenger, D., Raines, S. N., Libonate, S., Piche, F., Greenhouse, M. A., Smith, H. A., Thompson, K. L., Fischer, J., Woodward, C. E., & Hodge, T. 1995, ApJ, 448, 611
- Satyapal, S., Greenhouse, M. A., Luhman, M., fisher, J., Smith, H.A. 1997, BAAS, 191,2106
- Schaerer, D., Charbonnel, C., Meynet, G., Maeder, A., & Schaller, G. 1993a, A&AS, 102, 339
- Schaerer, D., Meynet, G., Maeder, A., & Schaller, G. 1993b, A&AS, 98, 523

- Schaller, G., Schaerer, D., Meynet, G., & Maeder, A. 1992, *A&AS*, 96, 269
- Schweizer, F. 1986, in *Nearly Normal Galaxies*, ed. S. Faber (New York: Springer), 18
- Searle, L., Sargent, W. L. W., & Bagnuolo, W. G. 1973, *ApJ*, 179, 427
- Schmutz, W., Leitherer, C., Gruenwald, R. 1992, *PASP*, 104, 1164
- Seiden, P. E., & Gerola, H. 1982, *Fund. of Cosmic Physics*, 7, 241
- Seiden, P.E., Schulman, L. S., & Gerola, H. 1979, *ApJ*, 232, 702
- Silk, J. 1997, *ApJ*, 481, 703
- Wynn-Williams, C. G., Hodapp, K. -W., Joseph, R. D., Eales, S. A., Becklin, E. E.,
McLean, I. S., Simons, D. A., & Wright, G. S. 1991, *ApJ*, 377, 426
- Zepf, S.E., Geisler, D., & Ashman, K.M. 1994, *ApJ*, 435, L117

Fig. 1.— BHK diagram. The colors were computed with the models of Leitherer et al. (1999) for the evolution of a coeval burst of star formation forming $10^6 M_{\odot}$ of stars distributed along a Salpeter initial mass function. Models with $\alpha = 2.35$, $M_{low} = 1 M_{\odot}$ and $M_{up} = 120 M_{\odot}$ and metallicities of 0.05 solar and solar are shown. The tracks are labeled from 0 to 10 Myr with 2 Myr time increments. The 0, 4 and 10 Myr time steps are shown. The extinction vector is shown on the left of the diagram.

Fig. 2.— Two color diagram diagram but this time with the (B–J) vs. (J–H) colors and solar metallicity only. The other parameters are the same as in Figure 1. Notice how the extinction vector and the old branch have a different alignment. Also, the difference between the young and old branches is much smaller than in the BHK diagram.

Fig. 3.— Double burst model. Two double burst models were explored. A double burst model with two bursts separated by 1 Myr (dashed; Model 1) and 3 Myr (dot dash; Model 2). The physical parameters of each double burst model are identical to those of the solar metallicity evolutionary path of Figure 1.

Fig. 4.— CFHT K band image of Arp 299. The bright regions are identified based on the convention of Wynn-Williams et al. (1991). North is up and east is left. The total field of view is $1' \times 1'$.

Fig. 5.— BHK color diagram of Arp 299. The solid curves are the theoretical model at 0.40 solar metallicity without dust emission (left) and considering a 0.2 mag increase in K magnitude due to dust emission (right). The observed points shown are those brighter than $M_B = -10$ and $M_K = -14$. The observations have been corrected for $E(B-V) = 0.16$. For these colors, the extinction vector is parallel to the old branch.

Fig. 6.— SSC age distribution in Arp 299. The age map (greyscale) is shown superposed to the contours of the B image. In this picture, region A, B1 and C are the youngest (< 4

Myr) while region B2 is the oldest (7-10 Myr). Notice that object B1 does not show up in the B image while it is the brightest in K. North is up and east is left. The extent of the whole image is ~ 12 kpc at the assumed distance of 42 Mpc.

Fig. 7.— Contour map of $EW(H\alpha)$ superposed on the wide R band image of NGC 3690. The highest region of $EW(H\alpha)$ is coincident with object C, confirming the results of the BHK diagram analysis. Each point on this image is a fiber of $0.4''$ for a total field of view of $12'' \times 10''$. Contours are labeled with surface $EW(H\alpha)$ values ranging from 5 to 53 \AA . North is up and east is left.

Table 1. Observations log

Band	Number of exposures	Exposure time(s)	Plate scale("'/pix)	Dispersion ($\text{\AA}/\text{pix}$)	FWHM psf (\AA)
OMM imaging					
B	3	3000	0.31	...	1.21''
V	3	1000	0.31	...	0.97''
R	3	500	0.31	...	0.90''
I	3	500	0.31	...	1.00''
CFHT IR imaging					
J	4	1 \times 60	0.314	...	0.9''
H	4	6 \times 20	0.314	...	0.9''
K	4	9 \times 20	0.314	...	0.9''
CFHT Spectroscopy					
3600-7000 \AA	3	3000	0.4	2.2	8 \AA

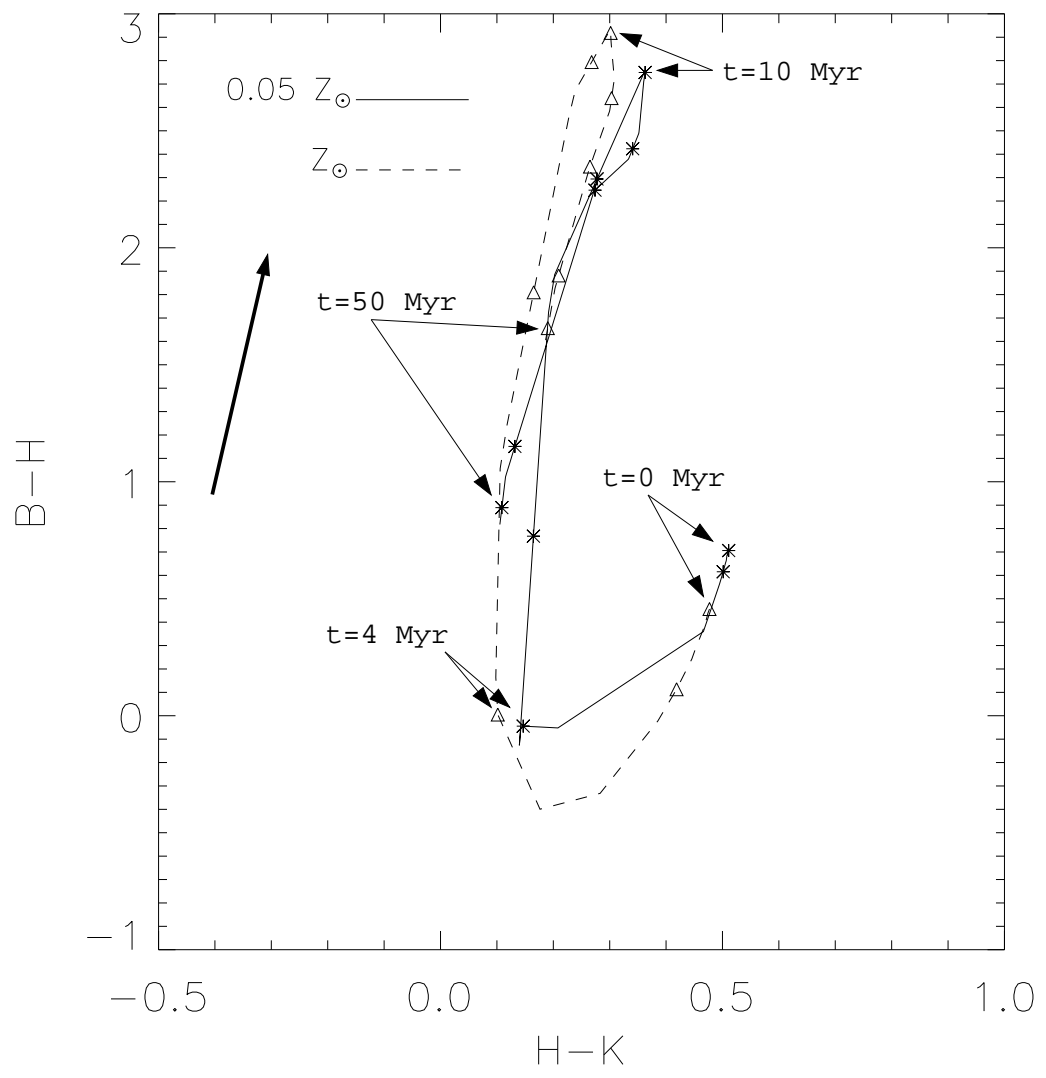


Fig. 1.—

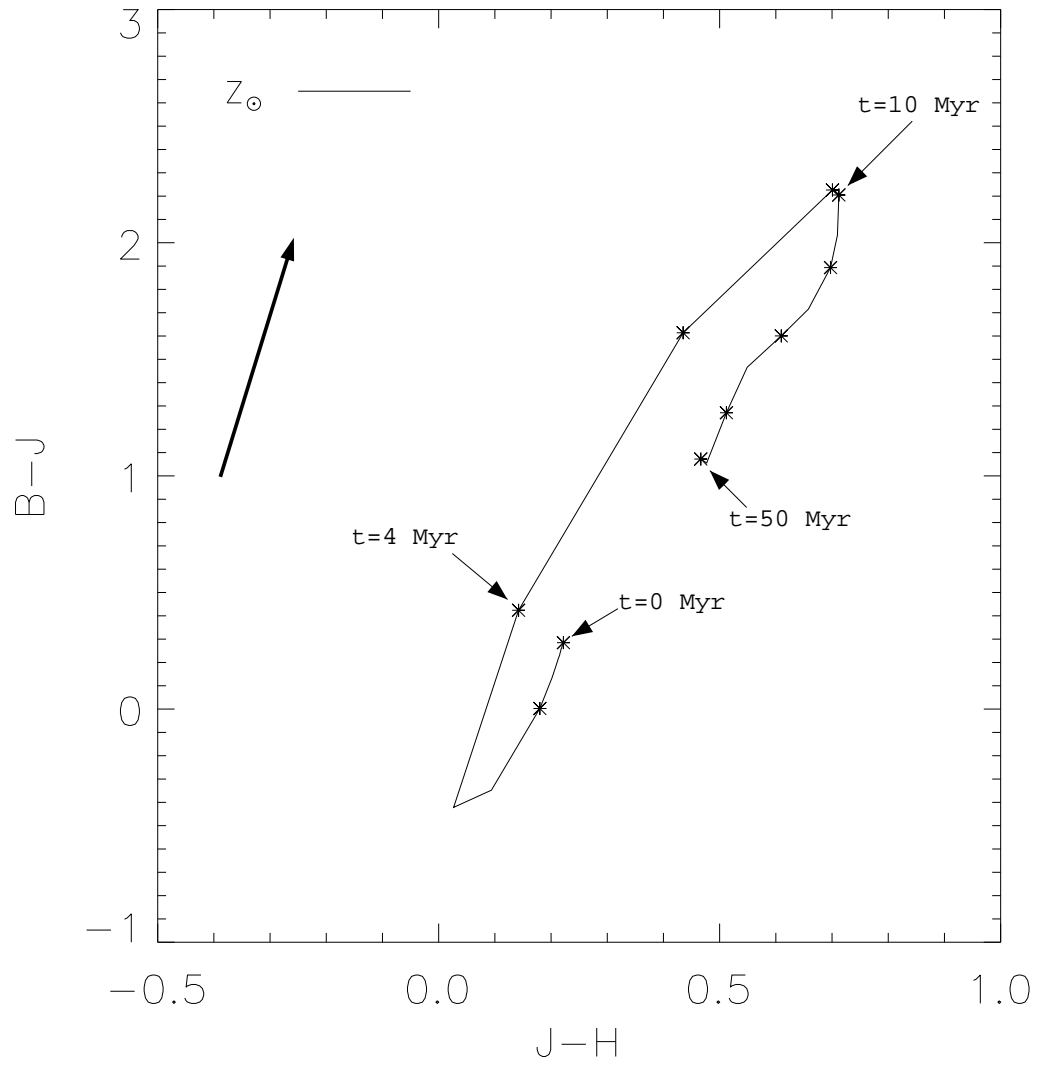


Fig. 2.—

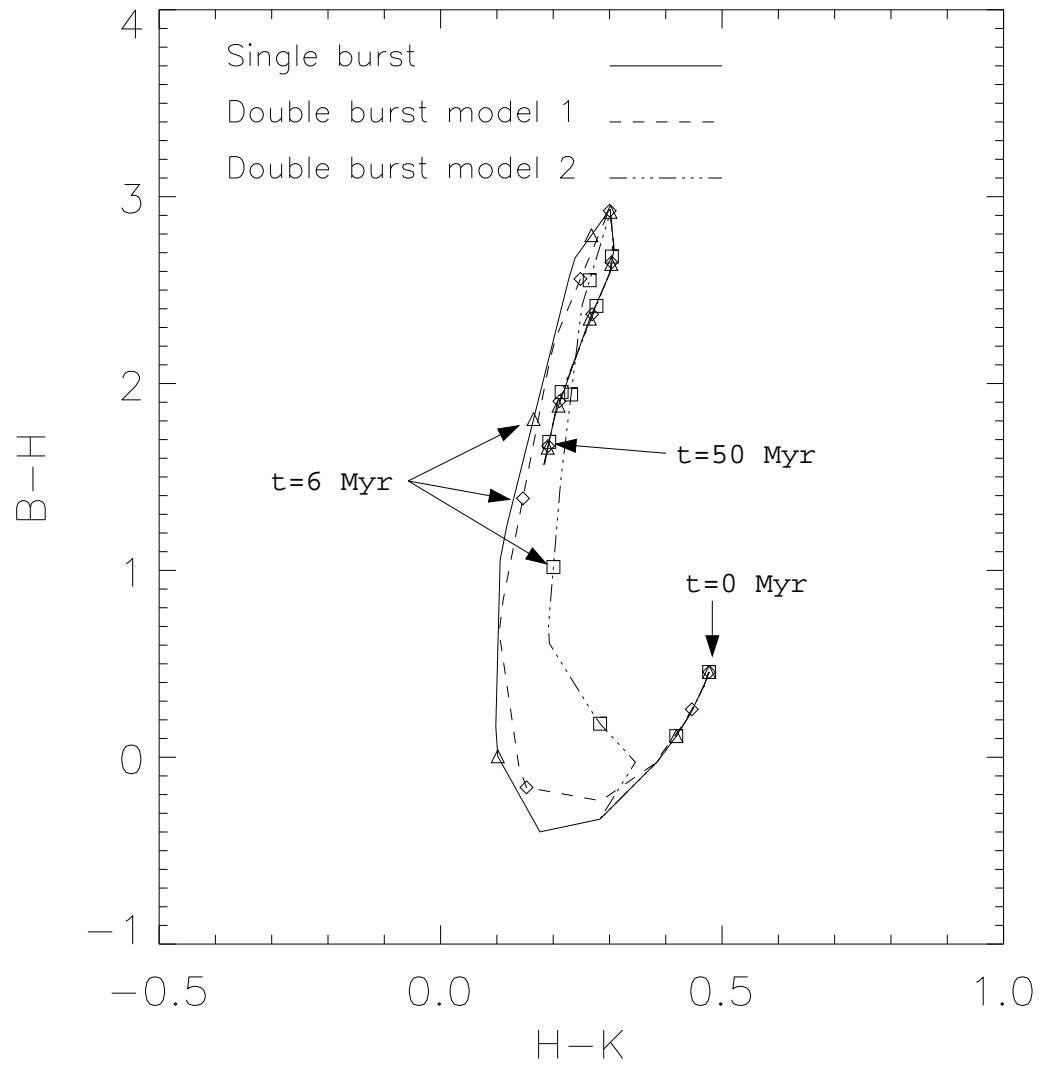


Fig. 3.—

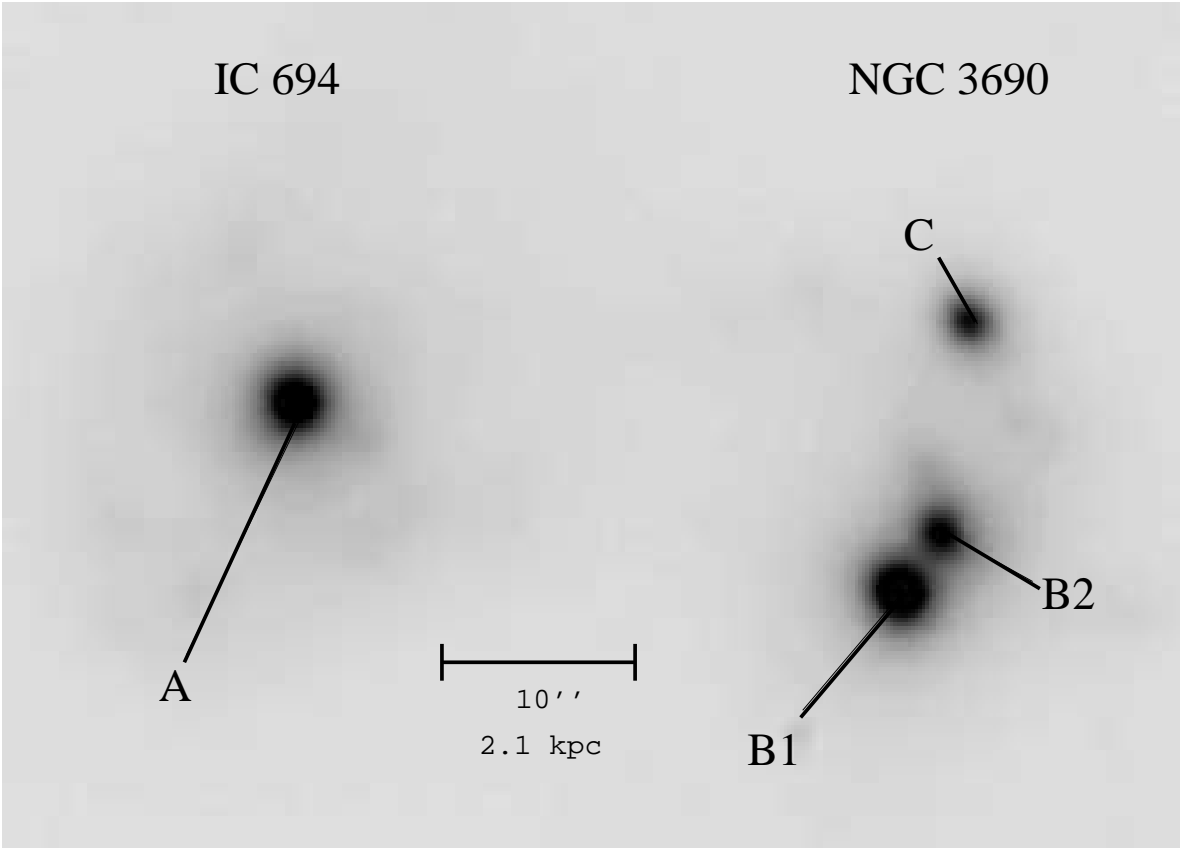


Fig. 4.—

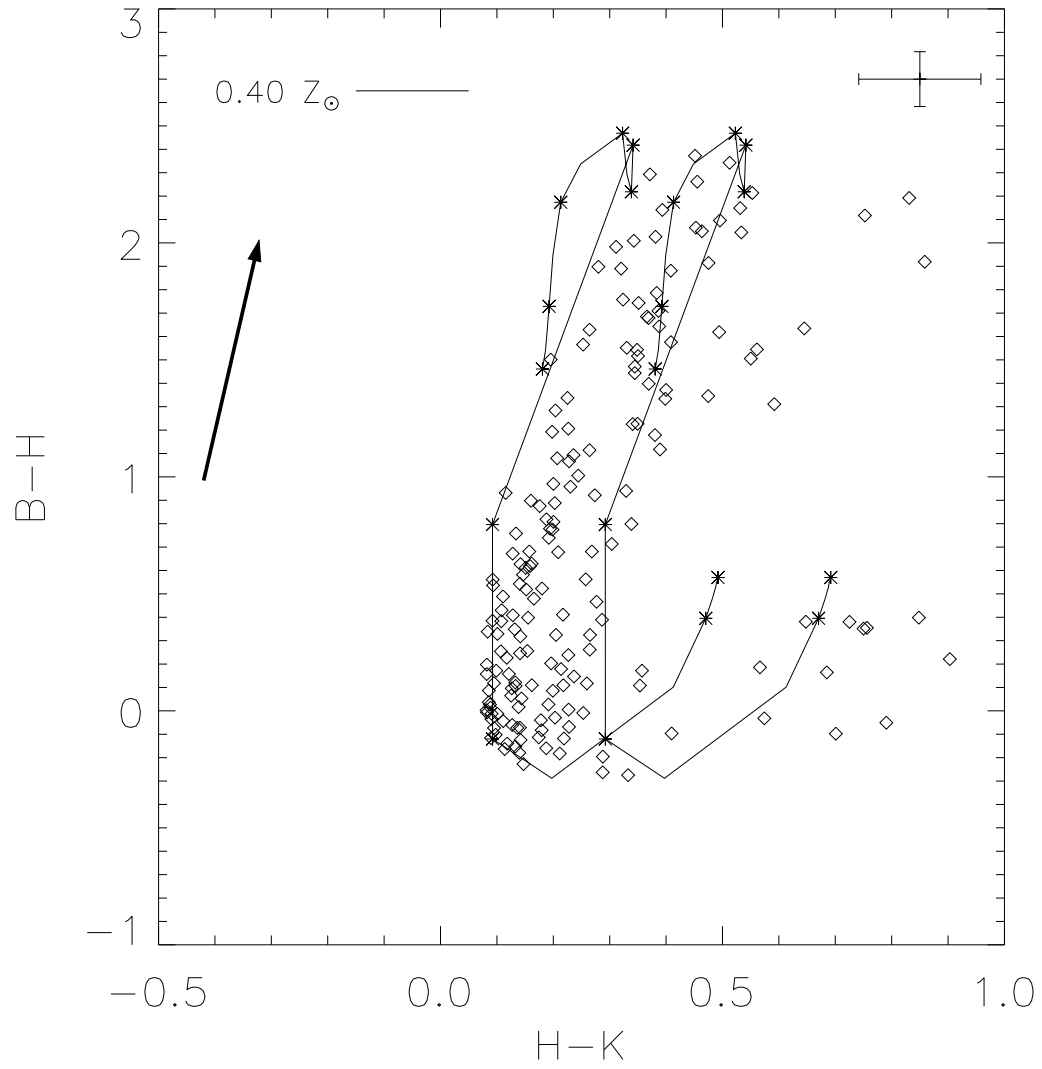


Fig. 5.—

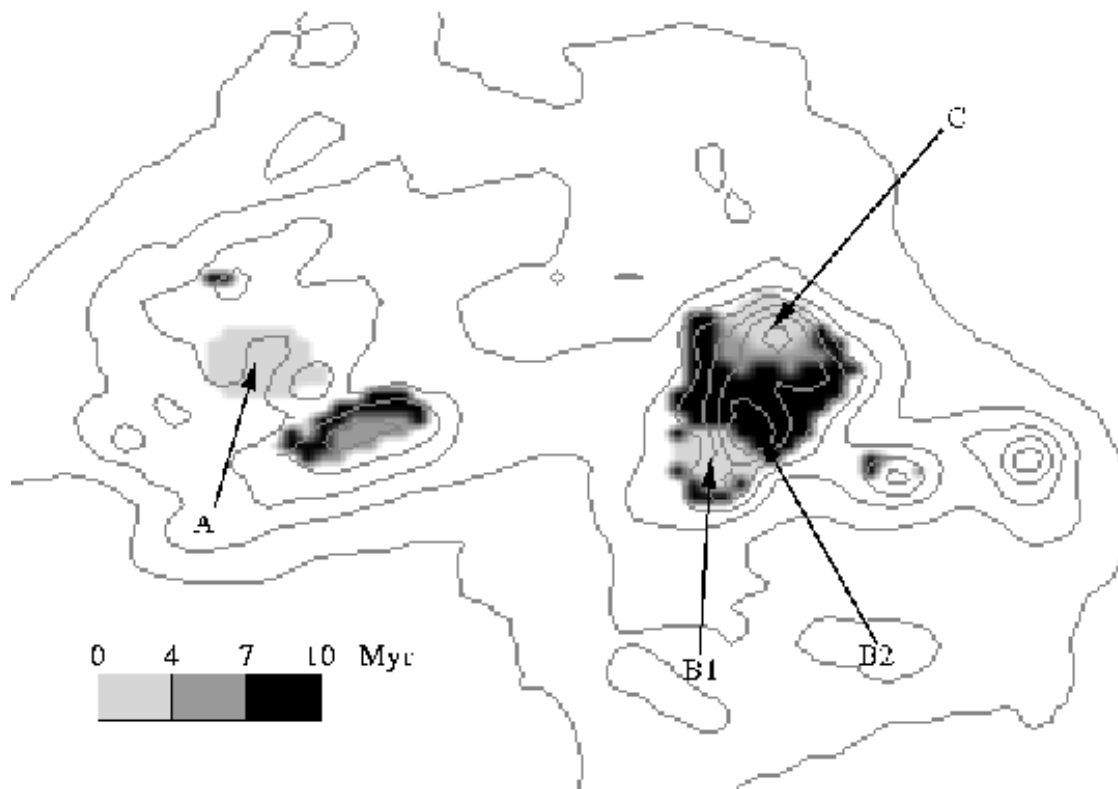


Fig. 6.—

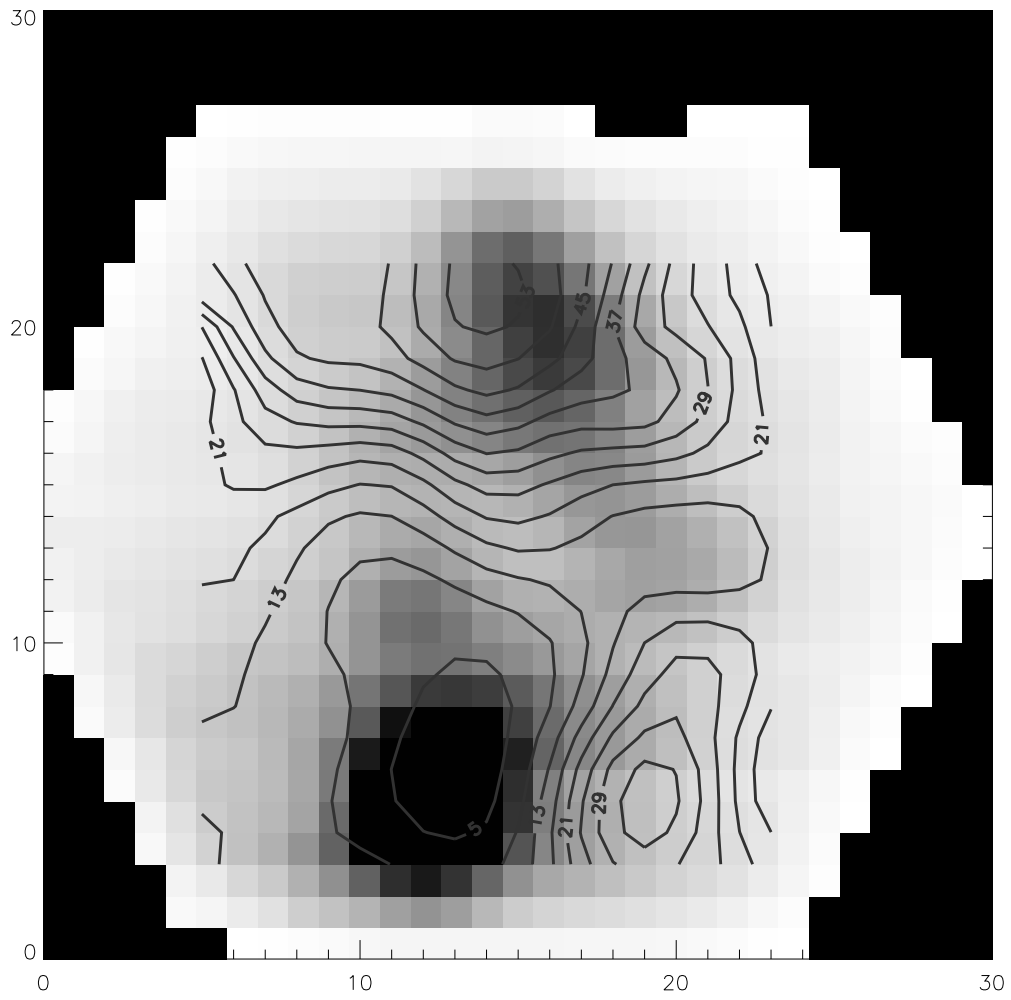


Fig. 7.—